A Steradian of the Southern Sky at 151.5 MHz From the Mauritius Radio Telescope

V.N.Pandey[1], **N. Udaya Shankar**[2] ([1,2]*Raman Research Institute*, Bangalore, India)
e-mail: *vnpandey@rri.res.in*[1] , *uday@rri.res.in*[2]

Abstract. We present a few results of a low frequency southern sky survey carried out using the Mauritius Radio Telescope (MRT). We present and discuss images at 151.5 MHz which form a part of wide field images covering one Steradian of the sky ($18^h \leq$RA$\leq 24^h$, -70°$\leq \delta \leq$-10°). A comparative study with a few other southern sky surveys is discussed. A source catalog of ≈3,000 radio sources has been constructed from the images. We discuss a few of the challenging aspects of imaging with the MRT namely, deconvolution of wide field images made using a non coplanar array like MRT and a novel framework developed for automatic evaluation of data quality for the survey.

1 Introduction

MRT is a Fourier synthesis, non-coplanar ⊤- shaped array with an East-West (EW) arm of length 2048 m having 1024 fixed helices, and a South arm of length 880 m consisting of a rail line on which 16 movable trolleys each with four helical antennas are placed [1]. The primary objective of this telescope is to carry out a survey of the southern sky ($00^h \leq$RA$\leq 24^h$, -70°$\leq \delta \leq$-10°). The low frequency spectrum of radio astronomy remains the most poorly explored regions of the electromagnetic spectrum despite its great scientific potential. The genesis for mapping the southern sky at metre wavelengths with the MRT was motivated due to the existing lacuna at low frequencies in the southern sky. In this paper we present some results of imaging of one Steradian of the southern sky. In Sect. 2 we briefly discuss a few of the interesting aspects of imaging with the MRT. Sect. 3 presents and discusses the wide field images. In Sect. 4 we summarize the overall results.

2 Imaging with the MRT

During the period from May, 1994 to March, 1999 more than 20,000 hours of astronomical observations have been carried out for the survey. MRT measures different Fourier components of the brightness distribution of the sky in 63 different set of configuration of the trolleys in the North-South (NS) arm over a period of time in order to sample baselines in the NS every 1 m. The visibilities are measured with four different delay settings to minimize the effect of bandwidth decorrelation. For each delay setting a small part of the sky in declination can be observed without appreciable decorrelation which is referred as a delay zone [2]. The imaging has been accomplished using the in-house developed software, **MA**u**R**itius **M**inimum **O**perating **S**ystem for **A**rray **T**elescopes (MARMOSAT) [1]. Many aspects of imaging with the MRT are very special due to its non-coplanarity [3]. Here we very briefly focus on concepts behind two of the interesting aspects - automatic evaluation of quality of astronomical data and deconvolution of the wide field images with the MRT.

2.1 Automatic Evaluation of Data Quality

The advancement in technology, quest for higher angular resolution and sensitivity is fueling rapid growth of data in astronomy. The raw database of the visibilities for the MRT survey has a total size of ≈ 1 Terabyte and consists of ≈20,000 hours of astronomical observations. We have developed an algorithm for automatic scientific classification of the visibility data depending on its quality and usefulness for imaging, and rank it in decreasing order of quality [4]. Quantification of quality of data is difficult since there is no unique way to define it [5]. The framework is based on the key parameters which affect the data quality namely the interference statistics, noise in the observed visibilities and strength and position of the Sun at the time of observation. To a visibility file for each key parameter, a numerical index is assigned which is called the Quality Factor (QF). The overall quality of a visibility file is calculated using the QFs assigned based on each parameter and the quality of the available calibration file. Thresholding is applied as an upper cutoff on the QFs based on individual key parameters for a data file to be accepted for imaging. At the heart of the entire data quality evaluation process is a stand alone computer program written in **Perl**, which accomplishes data classification automatically without any manual intervention.

We compared our results with that of the traditional approach based on human expertise using two schemes on about 500 visibility files. In the first scheme each data file was classified in three categories namely: good data - acceptable for imaging, poor data - which is doubtful, and bad data - to be rejected. The comparison between the human and automatic classification agrees in more than 85% of the cases. In the second scheme the data files were ranked in relative order of quality. On an average within a difference in the relative ranks of ±1 the agreement is 80%. The agreement is 91% when the difference of the relative ranks is ±2. A careful analysis of discrepant cases revealed that in most cases the automatic ranking was more appropriate. The comparison very clearly proves that the automatic scheme is efficient and reliable. This data evaluation scheme has been used for selecting good data for imaging. This has brought down the time required for imaging from a few days to a few hours.

2.2 Deconvolution of Wide Field Images

The images are synthesized on a sidereal hour basis to facilitate automation of data processing. At MRT we carry out meridian transit imaging [2] and the 2-D image is formed by stacking the 1-D images on the meridian for the observable range of declination at different sidereal times. MRT is highly non-coplanar with a maximum height difference of 35 m in the EW array. For each delay zone the raw images are synthesized for ≈30° in declination in order to obtain a deconvolved image of ≈15°. A simple application of Clarke's thumb rule, shows that the maximum declination range which can be

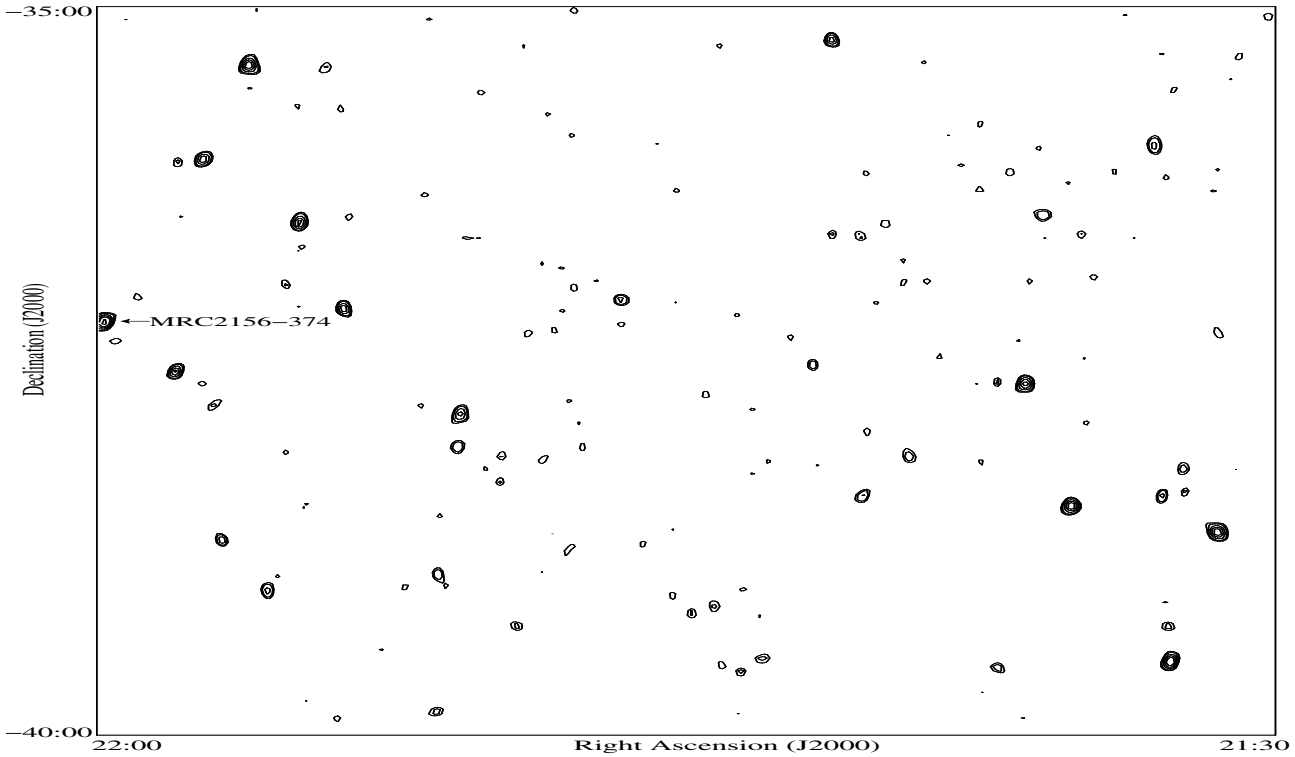

Figure 1: A sample wide field deconvolved image from the MRT survey with a resolution of $4' \sec(\delta) \times 4\farcm6 \sec(\delta+20\fdg14)$. The contour levels are 3, 5, 7, 10, 14, 25, 40 $\times$ rms(σ) which is 120 mJy beam^{-1}. There are 42 sources detected in this image above 5σ. The strongest source is MRC2156-374 (21:59:52,-37:10:38 - J2000) which has a flux density of 3.7 Jy.

treated as one facet in polyhedron imaging is about $\approx 2^\circ$. Due to these difficulties the calibrated visibilities are phased for each point in the sky on the meridian[2].

Due to non-coplanarity, the Point Spread Function (PSF) becomes declination dependent [6, 7, 8]. This difficulty is further compounded by the declination dependence of the bandwidth decorrelation and natural stretching of the Full Width Half Maximum (FWHM) of the beam in RA by $sec(\delta)$. For deconvolving the wide field images ($30^\circ \times 30^\circ$) at MRT of a given delay zone, we generate PSFs (extent $\approx 8^\circ \times 10^\circ$) at specifically chosen declinations such that the maximum error by approximating the PSF at any declination, with the closest available PSF is <0.2%. This approach has some similarities with the 'beam set' approach [9]. Additionally the positions of bright sources having flux densities above a threshold limit are estimated from the raw images and PSFs (extent $\approx 16^\circ \times 20^\circ$) are generated at those declinations. The generated PSFs are stored as a data bank on the hard drive. The deconvolution is carried out using Högbom CLEAN [10], and the deconvolved image produced has a size of $\approx 15^\circ \times 15^\circ$. During the deconvolution the algorithm approximates the PSF at the current detected peak position by the closest available PSF. This avoids the need for PSF interpolation in the image plane. The deconvolution program is equipped with a Graphical User Interface which has provision for masking regions affected by artifacts. These forbidden regions are not considered for searching the peaks during the CLEAN. The images have been CLEANed down to 5σ level with a loop gain of 0.05 and generally the number of iterations needed is in the range 10,000-15,000. Due to the uniform *uv* coverage generally the process of CLEAN is trouble free. The achieved dynamic range is approximately 70. Since the PSF is that of a cross, the dynamic range is higher along the diagonals.

3 Wide Field Images

The specifications of the MRT images are given in Table 1. Fig. 4 shows a typical image from the MRT survey with a rms noise of 120 mJy beam^{-1}. The rms noise varies from 120 mJy beam^{-1} (RA 22^h-23^h) to 300 mJy beam^{-1} (RA 18^h-19^h) due to the change in brightness temperature of the sky. A hierarchical scheme for Radio Frequency Interference (RFI) mitigation has been developed for imaging with the MRT [11]. Careful examination of the image indicates that there is no significant interference left in our final images. We also did not see any significant effects of ionospheric scintillations in our images.

The images were analyzed for flux and positional accuracies. For this purpose we used Molonglo Reference Catalog (MRC) at 408 MHz [12]. Assuming a spectral index ($S \propto \nu^{-\alpha}$, where S is the flux density, ν is the frequency and α is the spectral index) of -0.7, the lower flux limit of 0.6 Jy of MRC scales to 1.2 Jy at 151.5 MHz, so we expect to detect almost all the MRC sources in the area of overlap. The region of overlap has ≈1600 sources in the MRC source list. We searched around the expected position of these sources in our raw images and carried out a non linear fitting using Levenberg-Marquardt method using the expected beam. Source position in RA and declination, its peak flux density, beam widths in RA and declination, and background were used as free parameters during the fitting. We were able to detect 95% of the MRC sources with 5σ detection in our images. The comaparison of the fluxes and the spectral index distribution obtained is shown in Fig. 2. The spectral index distribution peaks around -0.75. The positional uncertainity

Frequency	151.5 MHz
Bandwidth	1 MHz
Declination Range	-70°≤ δ ≤-10°
RA span	18^h ≤RA≤24^h
Typical image size	15°×15°
rms level (1σ)	≈120-300 mJy beam^{-1}
Resolution	$4' \times 4'.6\ sec\ (\delta + 20^\circ.14)$
Polarization	Right circular (IEEE)

Table 1: Characteristics of MRT images

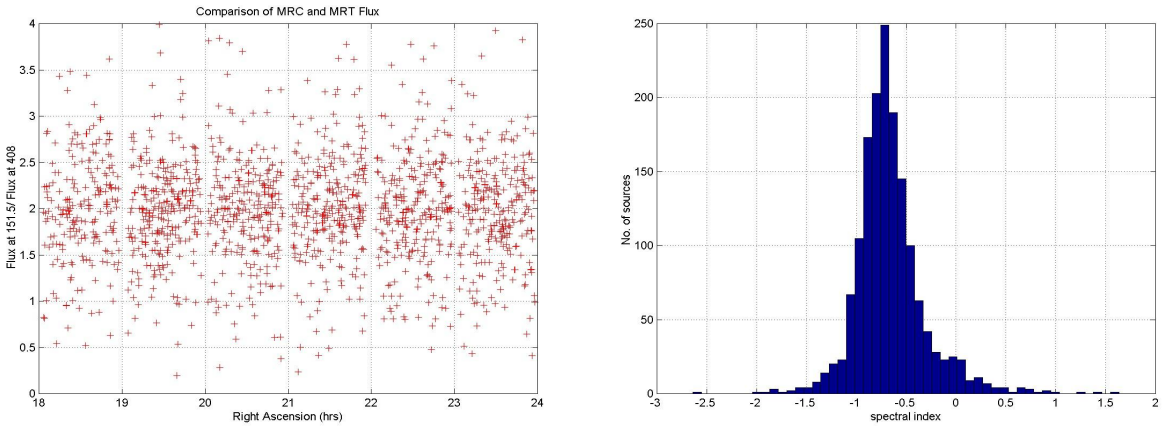

Figure 2: The figure on the left shows the ratio of the flux densities estimated from the MRT images and the MRC (408 MHz) for ≈1500 common sources (marked as +) detected in the images. The figure on the right shows the distribution of spectral indices obtained from the flux comparison.

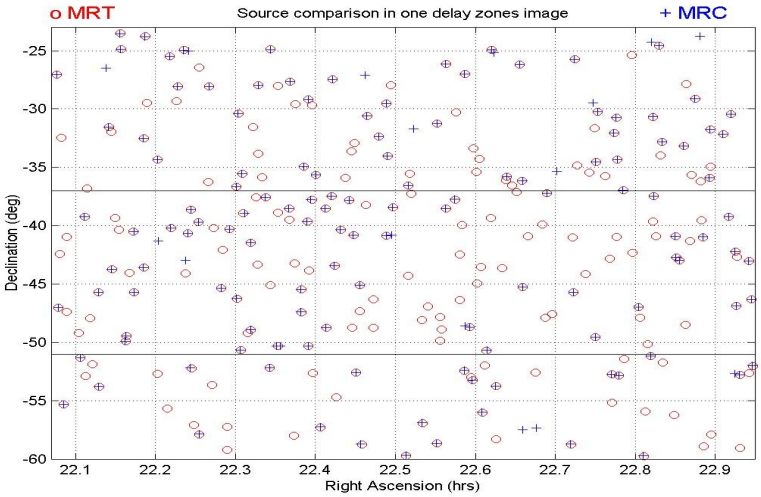

Figure 3: Plot showing the positions of 252 sources detected in a wide field MRT image (o) and the 133 sources listed in the MRC catalog (+).

for strong sources (>10σ) is about $\frac{1}{20}^{th}$ and $\frac{1}{10}^{th}$ of the beam widths (FWHM) in RA and declination. The uncertainity for weaker sources is affected by the rms noise and increases up to $\frac{1}{5}^{th}$ of the beam widths.

An algorithm has been developed for extracting the sources from the MRT images. A source catalog of ≈3,000 (5σ) unresolved and extended radio sources has been constructed from the images. The Fig. 3 shows the positions of the sources detected in a typical image, along with the sources in the MRC catalog. Details of the developed procedure would be discussed in a forthcoming paper. A list of steep spectrum sources has been prepared from the comparison for further investigation. Comparison of the MRT sources with the other catalogs like Parkes-MIT-NRAO (PMN) is under progress. Cross identification of sources in our images at other wavelengths using optical catalogs and IRAS sources will be carried out in the near future.

Due to availability of short spacings and nearly complete *uv* coverage, our images are sensitive to extended sources like Supernova Remnants (SNRs) which are generally objects of typical size 10′, with a typical surface brightness of ≈1.5×10^{-20}W m^{-2} Hz^{-1} Sr^{-1}(at 150 MHz) [13]. Our images are well suited to study their morphology, spectra and distinguish them from thermal sources like HII regions. An additional 0.5 Steradian of the sky (15^h≤RA≤18^h, -70°≤ δ ≤-10°) which includes a major part of the southern Galactic plane including the Galactic center has been imaged. Analysis of the Galactic plane imaged is under progress. The surface brightness sensitivity achieved in our images is ≈ 3.5×10^{-21}W m^{-2} Hz^{-1} Sr^{-1} (3σ). With this sensitivity we have been able detect and identify about 60 SNRs out of 80

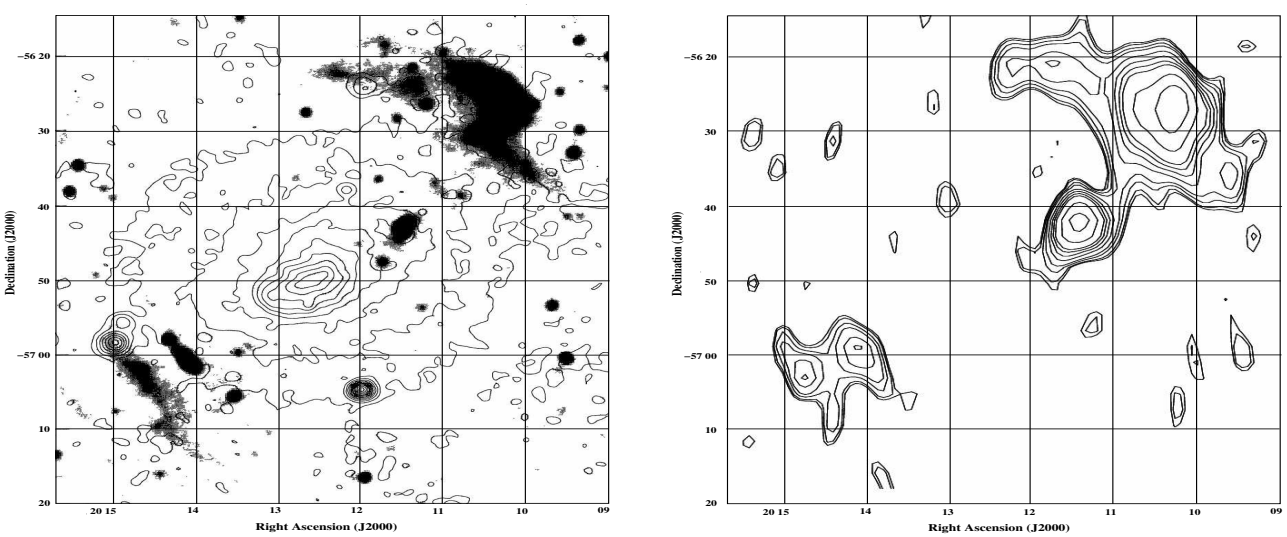

Figure 4: Image of the region around the cluster Abell 3667. The figure on the left shows a contour representation of the ROSAT PSPC image (0.1-2 Kev), overlaid on a grey scale radio image at 843 MHz from the MOST. The X-ray contours are set at $2, 8, 18, 32, 50, 72, 98, 128, 162, 200$ and $242 \times$ the background noise [17]. The MRT image of the same region on the right shows the extended emission suspected to be due to the shocks formed between the infalling matter and the cluster core. The contour levels are $3, 4, 5, 7, 10, 14, 20, 28, 40, 56, 80 \times \text{rms}(\sigma)$ which is ≈ 120 mJybeam^{-1}.

known in the literature in the region imaged. The images would be used to measure their integrated flux, and estimate their integrated spectra. Comparison of the images of a few extended SNRs from the literature at nearby frequencies confirmed that their morphology is well represented in our images.

Due to low frequency and surface brightness sensitivity, MRT is also suited for the study of extended extra-galactic sources such as Giant Radio Sources and relics. Cluster radio relics in the vicinity of clusters of galaxies are believed to be fossil galaxies, with shock accelerated relativistic electron population [14]. The necessary shock waves would be of Mpc scale and could be due to steady accretion of matter on to the cluster or due to merger event with another cluster. Recently observed sub-structures in X-ray temperatures maps support the existence of extended shock waves at locations of several known cluster relics [15, 16]. The Fig. 4 shows extended radio emission from these proposed shocks around the X-ray cluster Abell 3667 in the MRT image. A contour image from the ROSAT overlaid on a grey scale radio image at 843 MHz from the MOST is also shown [17]. These reactivated fossil galaxies are powerful tools to investigate the properties of infalling matter onto the clusters of galaxies and a test ground of large scale structure formation. These are steep spectrum sources and we expect to detect quite a few such sources in the MRT survey.

4 Conclusions

The algorithm developed for evaluation of data quality has made the data classification automatic, reliable and has brought down the time required for imaging from a few days to a few hours. With suitable modifications it has the potential to be used for other data sets in astronomy. A procedure for deconvolving wide field images made using a non coplanar array like MRT, has been successfully developed. A Steradian of the sky has been imaged and the analysis of the images presented, clearly demonstrate the success of the methods developed.

References

[1] Golap, K., Udaya Shankar, N., Sachdev, S., Dodson, R., & Sastry, Ch., V., 1998, JApa, 19, 35
[2] Sachdev, S., & Udaya Shankar, N., 2001, JApA, 22, 229
[3] Udaya Shankar, N., Golap, K., Sachdev, S., Dodson, R., Katwaroo, M., & Sastry, Ch.V., 2002, Ap&SS, 282, 15
[4] Pandey, V.N., Udaya Shankar, N., & Somanah, R., 2002, Ap&SS, 282, 29
[5] Sharpee, B., Williams, R., Baldwin, Jack A., van Hoof, & Peter A. M., ApJSS, 149, 157
[6] Golap, K., & Udaya Shankar, N., JApa, 22, 251
[7] Oozeer, N., & Udaya Shankar, N., 2002, Ap&SS, 282, 430
[8] Pandey, V.N., Oozeer, N., Udaya Shankar, N., & Somanah, R., 2002, Bull. Astron. Soc. India, 30, 773
[9] Waldram, E. M., & McGilchrist, M. M., 1990, MNRAS, 245, 532W
[10] Högbom, J., A., 1974, A&AS, 15, 417
[11] Pandey, V.N., & Udaya Shankar, N., URSIGA, 2005
[12] Large, M.L., Mills, B.Y., Little, A.G., Crawford, D.F., & Sutton, J.M., 1981, MNRAS, 194, 693
[13] Green, D.A., 2004, Bull. Astron. Soc. India, 32, 335
[14] EnBlin, T. A. & Biermann, P. L., 1998, A&A, 330, 90-96
[15] Markevitch, M., Forman, W. R., Sarazin, C. L., & Vikhlinin, A., 1998, ApJ, 503, 77-96
[16] Donnelly, R. H., et al. 1998, ApJ, 500, 138
[17] Röttgering, H. J. A., Wieringa, M. H., Hunstead, R. W., & Ekers, R. D., 1997, MNRAS, 290, 577